Bridge Damage Identification from Moving Load Induced Deflection Based on Wavelet Transform and Lipschitz Exponent

Zhu Yu, He Xia, José María Goicolea and Chaoyi Xia

The wavelet transform and Lipschitz exponent perform well in detecting signal singularity. With the bridge crack damage modeled as rotational springs based on fracture mechanics, the deflection time history of the beam under the moving load is determined with a numerical method. The continuous wavelet transformation (CWT) is applied to the deflection of the beam to identify the location of the damage, and the Lipschitz exponent is used to evaluate the damage degree. The influence of different damage degrees, multiple damage, different sensor locations, load velocity and load magnitude are studied. Besides, the feasibility of this method is verified by a model experiment.

Keywords: Wavelet transform; Lipschitz exponent; moving load; damage identification; experiment.

1. Introduction

Damage detection has been a subject of intensive investigation, since structural damage brings a serious threat to the service life and safety of a bridge. The main objective of damage detection is to identify the existence of any defect and to evaluate its location and degree. Vibration-based damage identification methods were proposed in the last century.[1,2] Since then, a large number of damage identification methods have been presented based on modal parameters, such as natural

frequencies and mode shapes. Although the modal parameters are easy to measure, it is difficult to extract from them the local information such as small defects. Besides, these parameters are affected by load, temperature and other environmental conditions, which tend to weaken the result derived.

Pandey introduced the modal curvature for damage detection, which was calculated from the structural displacement mode by the finite differences, and showed that it is more sensitive to damage than the mode shape itself.[3] Maia *et al.* identified the damage with the curvature frequency response function, derived from the displacement frequency response function.[4] Moreover, some other damage identification methods based on modal data such as modal strain energy method[5,6] were applied in damage identification. In the aforementioned methods, the damage indices are shown to be more effective, because they used the mathematical transformation of modal parameters rather than the original modal parameters. However, there are also some disadvantages, e.g. the result can be easily polluted by noise, and sometimes relies on the information of the undamaged structure.

In recent years, the wavelet transform has been introduced as a promising method in damage identification of structures, due to its excellent performance in detecting signal singularity. Numerous works exist on the wavelet-based damage identification.[7–13] These works present quite satisfactory results for damage location, but lack estimation of damage degree.

Hong *et al.* applied the wavelet transform to the displacement mode of a beam to locate the damage and introduced the Lipschitz exponent to estimate the damage degree.[14] Douka *et al.* estimated the size of the crack with an intensity factor, by relating the size of crack to the coefficients of the wavelet transform.[15] Beheshti-Aval *et al.* applied the wavelet transformation approach to damage identification using a harmonic class loading.[16] These methods, however, suffer from the lack of practicality, since they need many measuring points to obtain the detailed mode shape information.

Law *et al.* proposed a damage classification method based on the wavelet packet transform and statistical analysis, with good result achieved.[17] However, the bridge was excited by an impact load, which may not be applicable when the traffic is busy.

A beam under the moving load is a commonly used model in the dynamic analysis of bridges. Mahmoud studied the effect of cracks on the dynamic response of a simply supported beam subjected to a moving load or a moving mass.[18,19] Law and Zhu presented an experimental investigation on the dynamic behavior of a damaged concrete bridge under vehicular loads.[20] Zhu and Law[21] identified the bridge damage with the wavelet transform using the deflection time histories induced by the moving load. In their study, only a few measuring points were required, and they proved that the damage localization result is not sensitive to measurement noise. However, the proposed damage degree index needs the information of the intact bridge, while it may be difficult to obtain in practice. Besides, in their experiment, the damage was localized but not quantified, and the experiment result was not compared with the calculated one. Moreover, in their work, the damage was basically localized by the wavelet coefficient of one scale which cannot reflect the information of all the scales.

Zhan *et al.* proposed a damage detection method based on the train-induced bridge response and sensitivity analysis.[22] However, this method is prone to be affected by accuracy of the finite element model and is not easy to achieve in practice.

There are some other published works on the wavelet-based damage identification from the response time histories of bridges under the moving load, with some fruitful results.[23–30] However, most of these researches were not verified by experiment and some of them did not estimate the damage degree.

In this paper, by combining and improving the methods of Hong *et al.* and Zhu and Law,[14,21] a new damage detection approach is presented for a bridge subjected to a moving load. This method takes the advantages of the two methods, i.e. Lipschitz exponent and damage detection based on moving load induced deflection time history. With the Wavelet Transform applied to the moving load induced response time history of the bridge, the damage is localized by the 3D contour plots of the wavelet coefficient and the locus of maximum modulus of the wavelet coefficients, while the damage extent can be estimated by the Lipschitz exponent. This method has the following significant features: (a) The damage index has an explicit expression, and it is sensitive to local damage; (b) it uses the signal from only one or very few sensors; (c) it can identify the damage of the bridge from moving load induced deflections, so it can be conveniently adopted in field test; (d) it does not need the information of the intact bridge. Besides, this approach is verified by a more complete model experiment, in which not only the damage location, but also the damage extent is identified.

2. Analysis Model for a Damaged Beam Under Moving Load

Assume the bridge is a uniform Euler–Bernoulli beam with span L and the vehicle is modeled as a moving load $P(t)$ with velocity V, as shown in Fig. 1. The equation of motion can be written as

$$EI\frac{\partial^4 y(x,t)}{\partial x^4}+\rho A\frac{\partial^2 y(x,t)}{\partial t^2}+c\frac{\partial y(x,t)}{\partial t}=\delta(x-Vt)P(t), \tag{1}$$

where ρ, A and c are the density, cross-sectional area and damping of the beam, respectively, and δ is the Dirac function. The displacement $y(x,t)$ of the beam can be expressed in modal coordinates as

$$y(x,t)=\sum_{i=1}^{\infty} q_i(t)\phi_i(x), \tag{2}$$

where $\phi_i(x)$ is the ith mode shape function and $q_i(t)$ is the ith modal amplitude.

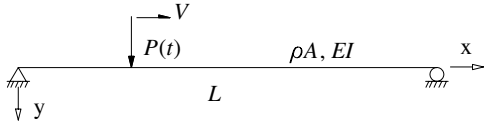

Fig. 1. A beam subjected to a moving load.

Substituting Eq. (2) in (1) and multiplying each term by $\phi_n(x)$, integrating with respect to x from 0 to L, and considering the orthogonality condition of mode shapes, we obtain

$$\frac{\mathrm{d}^2 q_i(t)}{\mathrm{d}t^2} + 2\xi_i\omega_i \frac{\mathrm{d}q_i(t)}{\mathrm{d}t} + \omega_i^2 q_i(t) = \frac{1}{M_i} P(t)\phi_i(Vt), \tag{3}$$

where ω_i, ξ_i, M_i are the frequency, damping ratio and mass of the ith mode. Once the mode shape function $\phi_i(x)$ is determined, the displacement $y(x,t)$ can be derived from Eq. (2) with $q_i(t)$ solved by integrating Eq. (3) numerically or analytically.

The crack damage of the beam is modeled as a rotational spring as shown in Fig. 2. According to the mechanics of fracture,[31] the stiffness of the rotational spring for a damaged beam section can be defined as $k_c = 1/C$, where

$$C = \frac{2H}{EI}\left(\frac{\lambda}{1-\lambda}\right)^2 [5.93 - 19.69\lambda + 37.14\lambda^2 - 35.84\lambda^3 + 13.12\lambda^4] \tag{4}$$

with λ denoting the ratio of crack depth h to beam height H. Since the rotational stiffness k_c is influenced by the parameter λ, it can be used to describe both single- and two-sided cracks.

For a single damage, the mode on the two sides of the damaged section can be expressed by two segmental functions as follows:

$$\phi(x) = \begin{cases} \phi_A(x) = A_1\sin(ax) + B_1\cos(ax) + C_1\sinh(ax) + D_1\cosh(ax) & (0 \le x < d) \\ \phi_B(x) = A_2\sin(ax) + B_2\cos(ax) + C_2\sinh(ax) + D_2\cosh(ax) & (d \le x \le L), \end{cases} \tag{5}$$

where d is the distance from the crack damage location to the left bearing of the beam; A_i, B_i, C_i, D_i $(i = 1, 2)$ are eight undetermined constants, and $a = \sqrt[4]{\omega^2\rho A/EI}$. The shape function $\phi_n(x)$ can be of any mode with $n = 1, 2, \ldots$, and correspondingly $a_n = \sqrt[4]{\omega_n^2\rho A/EI}$. The expression for multiple damage locations can be derived in a similar manner.

For the boundary conditions, the displacements and moments are zero at the two bearings, satisfying the following conditions:

$$\begin{cases} \phi_A(0) = 0, \\ \phi_B(L) = 0, \\ \phi''_A(0) = 0, \\ \phi''_B(L) = 0. \end{cases} \tag{6}$$

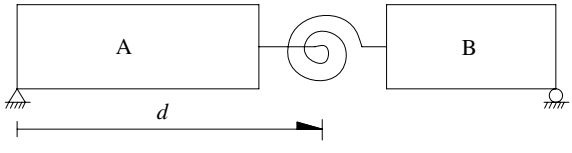

Fig. 2. Model of damage by rotational spring.

On the two sides of the damage location, the displacements, moments and shearing forces are continuous, while the rotational angles are discontinuous, namely,

$$\begin{cases} \phi_A(d) = \phi_B(d), \\ \phi'_A(d) = \phi'_B(d) + CEI\phi''_B(d), \\ \phi''_A(d) = \phi''_B(d), \\ \phi'''_A(d) = \phi'''_B(d), \end{cases} \tag{7}$$

where C was already given in Eq. (4).

Substituting Eq. (5) in (6) and (7), one can obtain eight equations for the coefficients A_i, B_i, C_i, D_i $(i = 1, 2)$. The compatibility condition for nontrivial solution of the equations is that the determinant of the coefficient matrix should be zero, namely,

$$\begin{vmatrix} 0 & 1 & 0 & 1 & 0 & 0 & 0 & 0 \\ 0 & -1 & 0 & 1 & 0 & 0 & 0 & 0 \\ 0 & 0 & 0 & 0 & s_1 & c_1 & \mathrm{sh}_1 & \mathrm{ch}_1 \\ 0 & 0 & 0 & 0 & -s_1 & -c_1 & \mathrm{sh}_1 & \mathrm{ch}_1 \\ s_2 & 0 & \mathrm{sh}_2 & 0 & -s_2 & -c_2 & -\mathrm{sh}_2 & -\mathrm{ch}_2 \\ c_2 - \eta s_2 & 0 & \mathrm{ch}_2 + \eta \mathrm{sh}_2 & 0 & -c_2 & s_2 & -\mathrm{ch}_2 & -\mathrm{sh}_2 \\ -s_2 & 0 & \mathrm{sh}_2 & 0 & s_2 & c_2 & -\mathrm{sh}_2 & -\mathrm{ch}_2 \\ -c_2 & 0 & \mathrm{ch}_2 & 0 & c_2 & -s_2 & -\mathrm{ch}_2 & -\mathrm{sh}_2 \end{vmatrix} = 0, \tag{8}$$

where $s_1 = \sin(aL)$, $c_1 = \cos(aL)$, $\mathrm{sh}_1 = \sinh(aL)$, $\mathrm{ch}_1 = \cosh(aL)$, $s_2 = \sin(as)$, $c_2 = \cos(as)$, $\mathrm{sh}_2 = \sin(as)$, $\mathrm{ch}_2 = \sin(as)$, $\eta = CEIa$. The preceding equation is an algebraic equation in terms of a. With the parameter a solved, the coefficients A_i, B_i, C_i, D_i $(i = 1, 2)$ can be obtained from Eqs. (6) and (7), and then the mode shape $\phi(x)$ from Eq. (5).

3. Damage Identification Using CWT and Lipschitz Exponent

For a signal $f(x)$, the continuous wavelet transform (CWT) is defined as[32,33]

$$\mathrm{W}[f(u,s)] = \frac{1}{\sqrt{s}} \int_{-\infty}^{\infty} f(x) \ {}^{*}\Big(\frac{x-u}{s}\Big) \mathrm{d}x, \tag{9}$$

where $\psi^*(x)$ is the complex conjugate of $\psi(x)$ which is a mother wavelet with dilation factor s and translation factor u, satisfying the admissibility condition:

$$\int_{-\infty}^{\infty} \frac{|\hat{\psi}(\omega)|^2}{|\omega|} \mathrm{d}\omega < \infty. \tag{10}$$

Here $\hat{\psi}(\omega)$ is the Fourier transform of $\psi(x)$. The existence of the integral in Eq. (10) requires

$$\hat{\psi}(0) = 0, \quad \text{i.e.} \int_{-\infty}^{\infty} (x)\mathrm{d}x = 0. \tag{11}$$

The CWT can be used to detect the signal singularity measured by the Lipschitz exponent, which can be defined as follows. A function f is said to be Lipschitz $\alpha \geq 0$ at $x = v$ if there exist $K > 0$ and a polynomial p_v of degree m (m is the largest integer satisfying $m \leq \alpha$) such that

$$f(x) = p_v(x) + \xi_v(x) \tag{12}$$

$$|\xi_v(x)| \leq K|x - v|^{\alpha} \tag{13}$$

The vanishing moment is important in applying the wavelet transform for the Lipschitz exponent. A wavelet $\psi(x)$ is said to have n vanishing moments if it satisfies

$$\int_{-\infty}^{\infty} x^k \psi(x) \mathrm{d}x = 0 \quad \text{for } 0 \leq k < n. \tag{14}$$

It may be shown that the wavelet having n vanishing moments is orthogonal to polynomials of up to degree $n - 1$. As a result of $\mathrm{W}[p_v(u, s)] = 0$, applying the CWT with $n \geq \alpha$ to the function of Eq. (12) yields

$$\mathrm{W}[f(u, s)] = \mathrm{W}[\xi_v(u, s)]. \tag{15}$$

Mallat[33] and Jaffard[34] show that if a square-integrable function $f(x)$ is Lipschitz $\alpha \leq n$ at $x = v$, the asymptotic behavior of the CWT near $x = v$ becomes

$$|\mathrm{W}[f(u, s)]| \leq A s^{\alpha+(1/2)} \left(1 + \left|\frac{u - v}{s}\right|^{\alpha}\right) \quad (A > 0). \tag{16}$$

Near the cone of influence of $x = v$, Eq. (16) reduces to

$$|\mathrm{W}[f(u, s)]| \leq A s^{\alpha+(1/2)}. \tag{17}$$

In Eq. (17), the high-amplitude wavelet coefficients are in the cone of the influence of singularity. The logarithmic form of Eq. (17) can be written as

$$\log_2 |\mathrm{W}[f(u, s)]| \leq \log_2 |A| + (\alpha + 1/2) \log_2 s, \tag{18}$$

where the logarithmic relationship between scale s and the maximum modulus $|\mathrm{W}[f]|_{\max}$ of the wavelet transform is linear with slope $k = \alpha + 1/2$. Then the Lipschitz exponent can be calculated as

$$\alpha = \frac{\log_2 |\mathrm{W}[f]|_{\max}}{\log_2 s} - \frac{1}{2}. \tag{19}$$

It is not difficult to see that the higher the singularity of the signal, the rougher the signal, and the smaller the Lipschitz exponent α. Hong *et al.*[14] concluded that for the mode shape of a damaged beam, the Lipschitz exponent where the damage locates between 1 and 2, namely,

$$1 < \alpha < 2 \tag{20}$$

and the greater the damage, the smaller the α.

Based on Eq. (20), the wavelet vanishing moments should be $n \geq 2$. Here the Mexican Hat Wavelet, which is the second derivative of the Gauss function $\theta(x)$, is employed with explicit expression as follows:

$$(x) = \frac{\mathrm{d}^2\theta(x)}{\mathrm{d}x^2} = \frac{2}{\sqrt{3\sigma}}\pi^{-1/4}\left(\frac{x^2}{\sigma^2} - 1\right)\exp\left(\frac{-x^2}{2\sigma^2}\right). \tag{21}$$

Zhu and Law[21] concluded that the mode information can be obtained from the deflection time history at one point of the beam subjected to moving load. On this basis, the procedure of damage identification can be listed as follows:

(1) Measure the deflection time history of the bridge under the moving load.
(2) Apply the wavelet transform to the deflection to obtain the wavelet coefficient.
(3) Localize the damage by the wavelet coefficient contour plot at different scales. Where there is a damage crack with singularity, there will appear a maximum value of the wavelet coefficient, thus there will be an obvious cone of influence at the damage location in the contour plot.
(4) Calculate the Lipschitz exponent α to estimate the damage extent. The greater the damage, the smaller the value α.

4. Numerical Example

The simply-supported beam concerned has a span of 50 m, with a cross-section 1.0-m high and 0.5-m wide, Young's modulus $E = 210\,\mathrm{GPa}$, and material density $\rho = 7860\,\mathrm{kg/m^3}$. The fundamental frequency calculated is $f_0 = 0.94\,\mathrm{Hz}$. The moving load is $P = 10\,\mathrm{kN}$ with velocity $V = 1\,\mathrm{m/s}$. The first six modes are considered in the analysis.

4.1. *Single damage*

Assume the damage is located at the midspan with different damage degrees $\lambda = 0$, 0.2 and 0.5 for comparison. Figure 3 shows the normalized dynamic deflection with

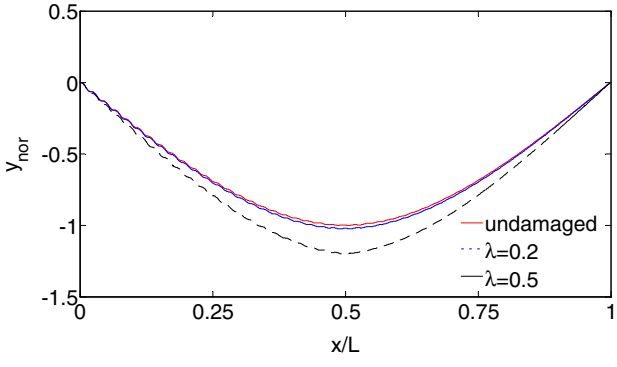

Fig. 3. Deflection time histories at midspan of beam under different damage degrees.

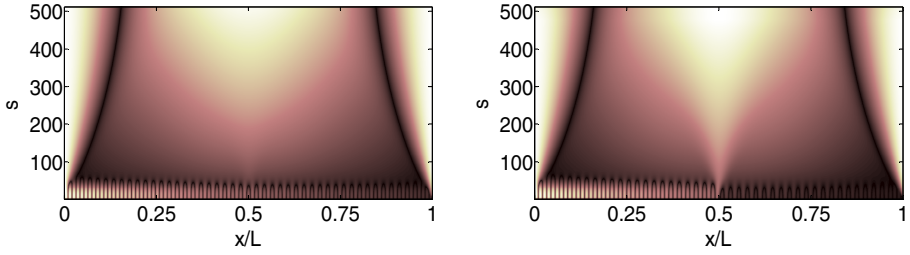

Fig. 4. Contour plots of $|\mathrm{W}[f]|$ with damage degree: (a) $\lambda = 0.2$ and (b) $\lambda = 0.5$.

respect to the normalized load location x/L. The normalized dynamic deflection y_{nor} is defined as the dynamic deflection relative to the midspan static deflection $\Delta = PL^3/(48EI)$. It should be noticed that the deflection increases with the damage, as expected.

Applying the CWT to the responses ($\lambda = 0.2$, $\lambda = 0.5$), the contour plots of wavelet transform modulus $|\mathrm{W}[f]|$ are shown in Fig. 4, where the Mexican Hat wavelet is used with scale $s = 512$. In the contour plot, the brighter the color is, the bigger the wavelet coefficient value it shows.

It can be seen that in any of the damage cases, there is a bright cone stripe at the damage position and the more serious the damage, the brighter the stripe. The loci of maximum moduli obtained from Fig. 4 are shown in Fig. 5. Both the loci lie around the midspan, which also locate the damage. Figure 6 shows the logarithmic relationship between $|\mathrm{W}[f]|_{\max}$ and s, from which the Lipschitz exponents are calculated to be

$$\alpha = \begin{cases} 1.8651 & (\lambda = 0.2) \\ 1.5501 & (\lambda = 0.5). \end{cases} \tag{22}$$

It can be seen that the deeper the damage crack, the smaller the Lipschitz exponent.

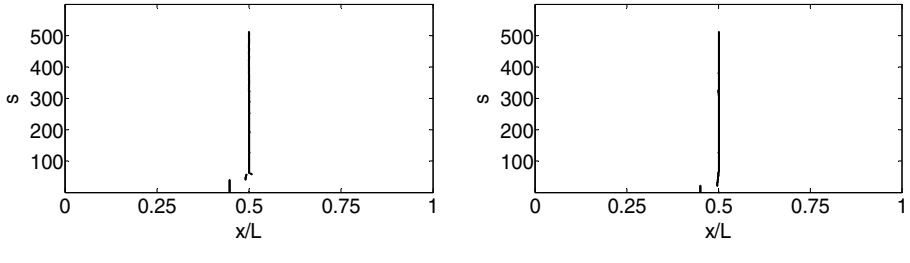

Fig. 5. Loci of maximum moduli $|\mathrm{W}[f]|_{\max}$: (a) $\lambda = 0.2$ and (b) $\lambda = 0.5$.

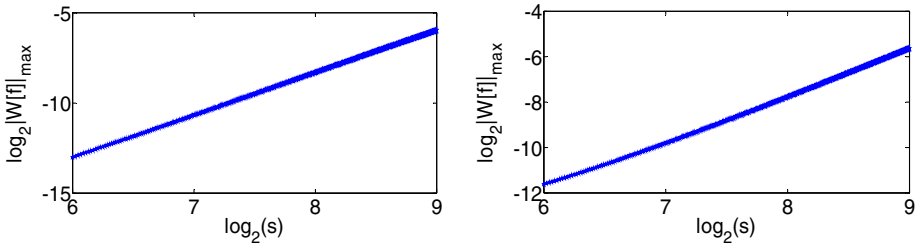

(a) (b)

Fig. 6. Logarithmic relationships between $|\mathrm{W}[f]|_{\max}$ and s: (a) $\lambda = 0.2$ and (b) $\lambda = 0.5$.

4.2. *Multiple damage with two cracks*

Assume that there are two cracks in the damaged beam, $\lambda = 0.3\,@\,1/4L$ and $\lambda = 0.5\,@\,1/2L$ with moving load velocity $V = 0.5\,\mathrm{m/s}$. The deflection history at both $1/4L$ and $1/2L$ are obtained and the calculation results are shown in Figs. 7 and 8. In Fig. 7, there appear two bright stripes at the two ends, which are due to the entry and exit of the moving load, as explained by Zhu and Law.[21] Figure 8 shows the loci of modulus maxima, which are extracted from the contour plots in Fig. 7.

It should be noticed that whatever the deflection at $1/4L$ or $1/2L$ is used, the two damages can be identified. Moreover, for the crack at $1/2L$, the stripe is brighter when the sensor is at $1/2L$ while for the crack at $1/4L$, the stripe is more obvious when the sensor is at $1/4L$, which shows the fact that it is easier to identify the damage when the sensor is near the damage area. That is because when the sensor is near the crack, the response is more affected by the damage, which will reveal a more intense singularity. As for Fig. 8(b), the loci of maximum moduli at $1/4L$ can be used to locate only the crack damage below the scale 75, since the damage at $1/4L$ is smaller and far away from the sensor. The Lipschitz exponents can be calculated as

$$\begin{aligned} \alpha_{1/4} &= 1.7682\,@\,1/4L \quad \alpha_{1/2} = 1.9917\,@\,1/4L \\ \alpha_{1/4} &= 1.4968\,@\,1/2L \quad \alpha_{1/2} = 1.3115\,@\,1/2L, \end{aligned} \tag{23}$$

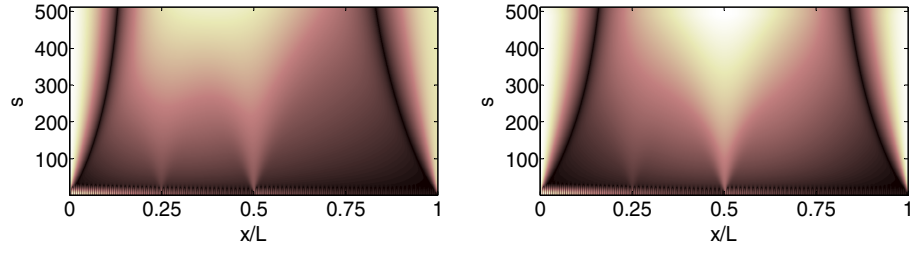

(a) (b)

Fig. 7. Contour plots of $|W[f]|$ with deflection of (a) $1/4L$ and (b) $1/2L$.

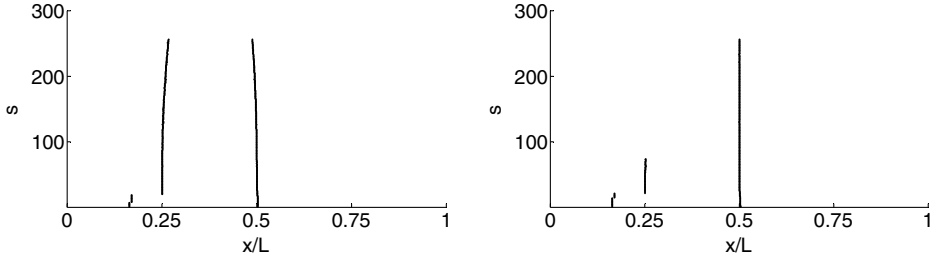

Fig. 8. Loci of maximum moduli $|\mathrm{W}[f]|_{\max}$ at (a) $1/4L$ and (b) $1/2L$.

where the subscript of α indicates the sensor location. From Eq. (23), we observe that $\alpha_{1/4} < \alpha_{1/2}\,@\,1/4L$ as well as $\alpha_{1/2} < \alpha_{1/4}\,@\,1/2L$ also verifies the rule above. Besides, $\alpha\,@\,1/4L > \alpha\,@\,1/2L$ indicates that the damage at $1/2L$ is more serious, as expected. Thus, although the damage degree identification is dependent on the sensor location, it can be relatively compared if there exists an additional sensor.

In Fig. 7, there appear some short bright stripes at the lower scale region, but they won't influence the identified result from the whole scale. In Fig. 8, the locus at 0.25 shifts a little to the left when the scale is smaller than 20, but the loci at all other scales indicate the position of damage at 0.25. This means that in the analysis, the locus of maximum modulus should be used to decide the damage for the entire scale.

4.3. *Effect of load velocity*

Again take the beam with a single damage ($\lambda = 0.5\,@\,1/2L$) for example, while three load velocities $V = 1$, 2 and 4 m/s are considered for comparison. The time histories of the normalized midspan deflection of the beam are shown in Fig. 9. It can be seen that the dynamic components increase with the loading velocity.

Shown in Fig. 10 are the contour plots of $|\mathrm{W}[f]|$ for the midspan deflections of the beam under three loading velocities. One can find that all the damage can be

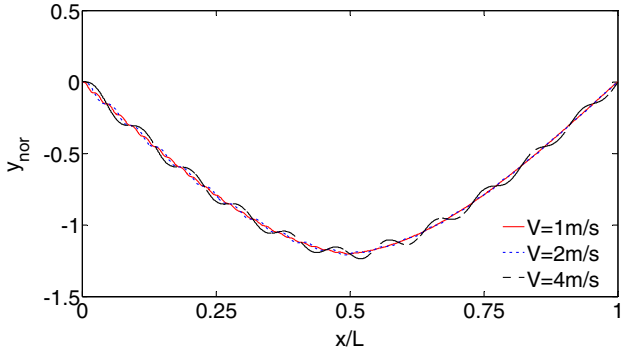

Fig. 9. Deflection time histories of midspan of beam under different velocities.

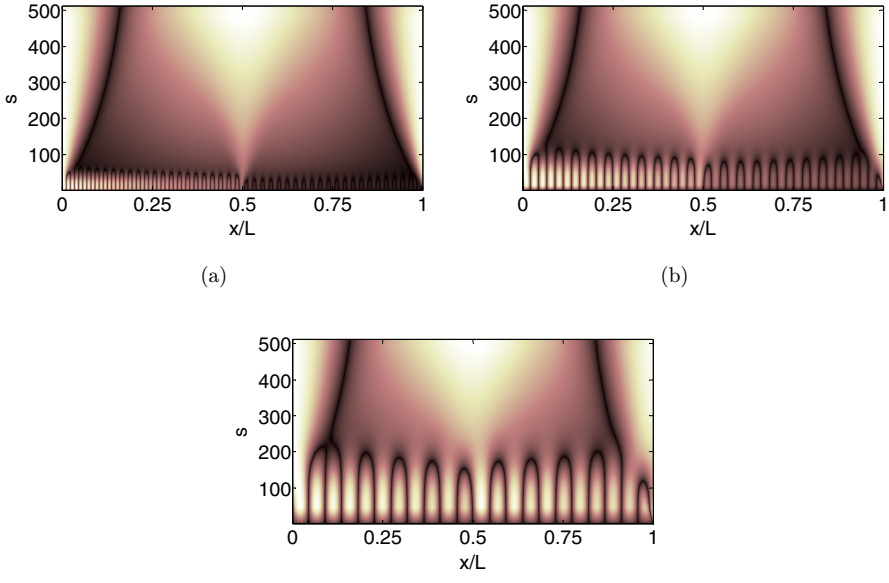

Fig. 10. Contour plots of $|\mathrm{W}[f]|$ under velocities of (a) 1 m/s, (b) 2 m/s and (c) 4 m/s.

identified, and the higher the velocity is, the more false bright stripes appear for the lower scales, which affects the identification of damage locations. For example, the damage location under velocity (c) can only be identified when the scale is higher than 200, because the dynamic components introduced by higher velocity contain more singularities in the contour plots.

4.4. *Effect of load magnitude*

The beam with a single damage ($\lambda = 0.5\,@\,1/2L$) is taken for example with different load magnitudes, i.e. $P = 10, 50$ and 100 kN. The midspan deflection time histories of

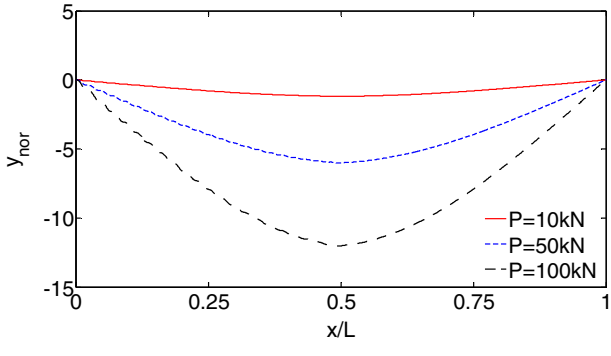

Fig. 11. Normalized deflection time histories of midspan of beam under different load magnitudes.

the beam under different load magnitudes (normalized to the static deformation under $P = 10\,\text{kN}$) are shown in Fig. 11. The result indicates that the amplitude of deflection increases with the increase in load magnitude, as expected. However, if the structure is still linearly elastic, the damage identification result is not much affected by the load magnitude, since the regularity of the signal remains unchanged. Whatever the load magnitude is, the result is almost the same as that of Figs. 4(b), 5(b) and 6(b) and the Lipschitz exponent α is the same as that in Eq. (22), that is, $\alpha = 1.5501$ ($\lambda = 0.5$).

5. Experimental Verification

To verify the damage detection method presented herein, a model test was performed, as shown in Fig. 12, using a steel simply-supported beam with span $L = 1900\,\text{mm}$, thickness $H = 20\,\text{mm}$, width $b = 140\,\text{mm}$, Young's modulus $E = 210\,\text{GPa}$, and density $\rho = 7860\,\text{kg/m}^3$. The fundamental frequency calculated is 12.99 Hz.

The damage was simulated by cutting off part of the beam section, with the depth of the damaged area equal to h and the width 60 mm. A wheel with adjustable weight ($m_1 = 2.9\,\text{kg}$, $m_2 = 5\,\text{kg}$) was used to simulate the moving load, which rolled on the beam. The wheel moved on the beam at a constant velocity V. Three deflection sensors were placed at $1/4L$, $1/2L$ and $3/4L$ of the beam, and the deflection time history under moving load is recorded with a sampling frequency of 1024 Hz.

Six damage scenarios were considered in the test, as shown in Table 1, including four single damaged beams and two double damaged beams. In each damage

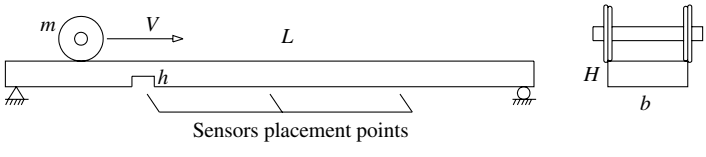

(a)

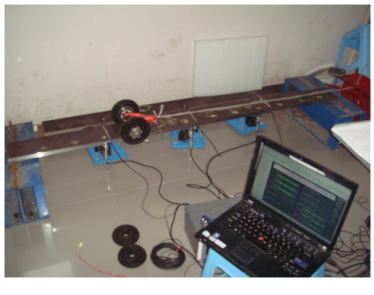

(b)

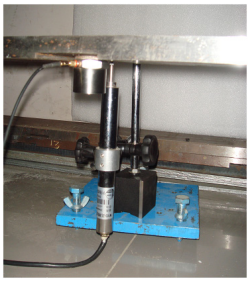

(c)

Fig. 12. Sketch of model test.

Table 1. Damage scenarios for test beam.

	Scenario No.	Damage location	Damage depth h (mm)
Single damage	Scenario 1	$3/4L$	5
	Scenario 2	$3/4L$	10
	Scenario 3	$1/2L$	5
	Scenario 4	$1/2L$	10
Multiple damages	Scenario 5	$1/2L + 3/4L$	$10 + 5$
	Scenario 6	$1/4L + 3/4L$	$10 + 5$

scenario, the beam was subjected to different wheel weights and different load velocities ($V_1 = 0.2\,\text{m/s}$, $V_2 = 0.3\,\text{m/s}$).

5.1. *Comparison with numerical results*

Take Scenario 1 for example, the deflection time history of $3/4L$ under load m_2 and velocity V_1 is calculated and compared with the experimental result, as shown in Fig. 13. The damage in the test beam was simulated by cutting off the section with some width ($0.735L$–$0.765L$) rather than just a crack with no width at $3/4L$ in the experiment. In contrast, three cracks are assumed to locate each at $0.74L$, $0.75L$ and $0.76L$ of the beam in the numerical simulation.

From the results shown in Fig. 13, it can be seen that in general, the numerical result agrees well with the experimental one, but it is a bit smaller. The reason is that although three cracks are used, the damage in the numerical model is still smaller than that in the experiment.

The CWT is applied to the response with Mexican Hat Wavelet and scale $s = 512$. The wavelet coefficient contour plot and locus of the maximum modulus of the calculated and measured results are shown in Figs. 14 and 15, respectively.

One can see that a bright stripe appears at $3/4L$ in Fig. 14 and so does the locus of $|\text{W}[f]|_{\max}$ in Fig. 15, which reveals the location of damage. Besides, the experimental

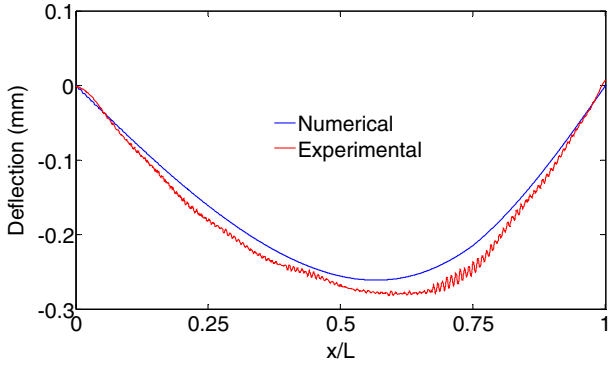

Fig. 13. Comparison of numerical and experimental deflection time histories at $3/4L$ of the beam.

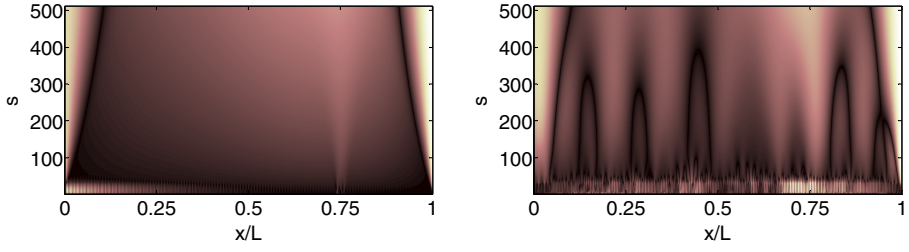

(a) (b)

Fig. 14. Contour plots of $|\mathrm{W}[f]|$: (a) Numerical result and (b) experimental result.

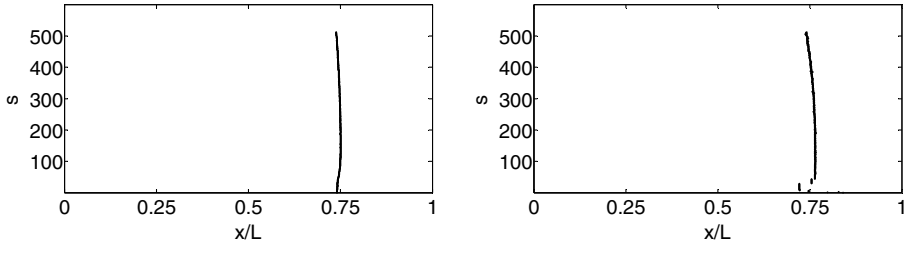

(a) (b)

Fig. 15. Locus of maximum modulus $|\mathrm{W}[f]|_{\max}$: (a) Numerical result and (b) experimental result.

result agrees well with numerical one, although the experimental result is influenced by environment noise to a certain degree in Fig. 14(b).

The logarithmic relationship between $|\mathrm{W}[f]|_{\max}$ and scale s is shown in Fig. 16, from which the Lipschitz exponents are obtained as $\alpha_{3/4} = 1.7214$ (numerical) and $\alpha_{3/4} = 1.3824$ (experimental). It is easy to understand that the numerical Lipschitz exponent is larger since the simulated damage is smaller than that in the test beam.

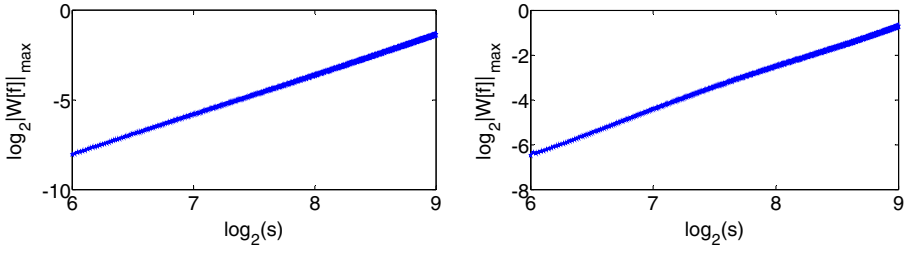

(a) (b)

Fig. 16. Logarithmic relationships between $|\mathrm{W}[f]|_{\max}$ and s: (a) Numerical and (b) experimental.

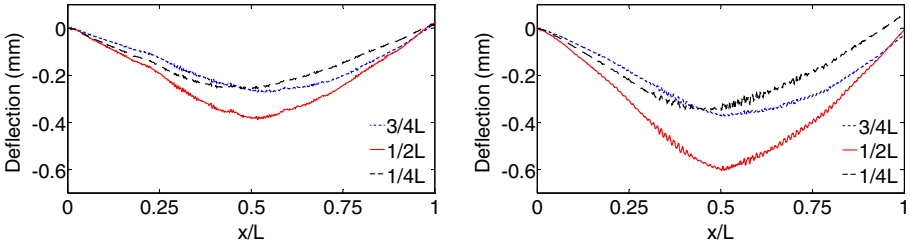

(a) (b)

Fig. 17. Deflection time histories of different sensors: (a) Scenario 3 ($h = 5\,\text{mm}$) and (b) Scenario 4 ($h = 10\,\text{mm}$).

5.2. *Effect of different damage degrees*

The effect of damage degree is studied by comparing Scenario 3 ($h = 5\,\text{mm}$) with Scenario 4 ($h = 10\,\text{mm}$), where m_2 and V_1 are considered. The deflections at $1/4L$, $1/2L$ and $3/4L$ are shown in Fig. 17. It can be seen that for Scenario 4 the maximum deflection is larger than Scenario 3 for whichever sensor position, since the damage in Scenario 4 is more serious, even though the damage locations are the same. Take the sensor at midspan of the beam for example, the damage identification results are shown in Figs. 18–20, and the Lipschitz exponents are calculated as $\alpha_{1/2} = 1.4565$ (Scenario 3) and $\alpha_{1/2} = 1.3355$ (Scenario 4).

It can be seen from Figs. 18 and 19 that the damage location in both scenarios can be identified. Moreover, in Fig. 18, the stripe at midspan of the beam for Scenario 4 is brighter, which shows that the damage is more serious. In Fig. 19 the damage for Scenario 3 can only be located after scale 248. In general, the more serious the damage is, the easier the damage can be identified. The Lipschitz exponent is smaller for larger damage, which is in accordance with the theoretical expectation.

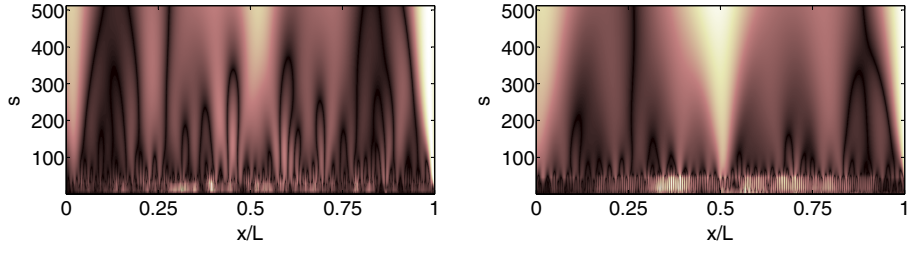

(a) (b)

Fig. 18. Contour plots of $|\mathrm{W}[f]|$ of midspan deflection: (a) Scenario 3 ($h = 5\,\text{mm}$) and (b) Scenario 4 ($h = 10\,\text{mm}$).

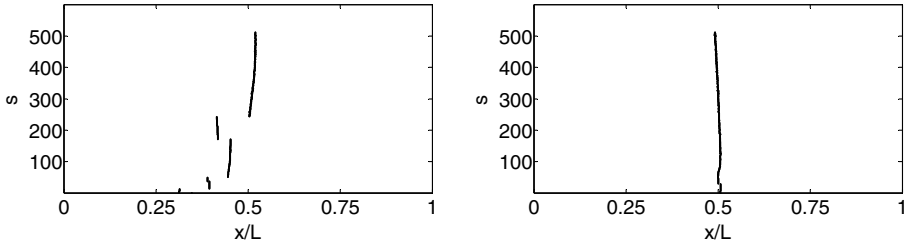

Fig. 19. Loci of maximum moduli $|\mathrm{W}[f]|_{\max}$: (a) Scenario 3 ($h = 5\,\mathrm{mm}$) and (b) Scenario 4 ($h = 10\,\mathrm{mm}$).

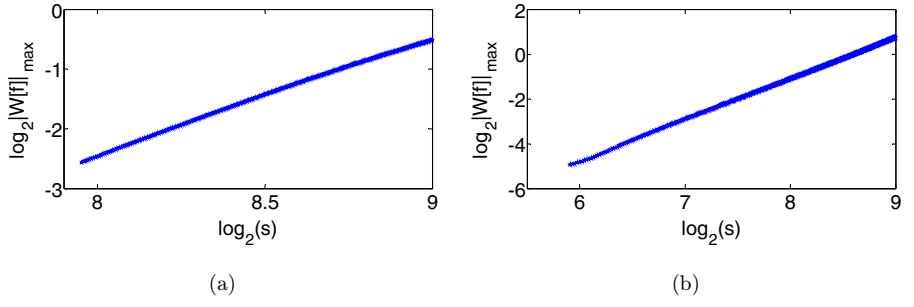

Fig. 20. Logarithmic relationships between $|\mathrm{W}[f]|_{\max}$ and s: (a) Scenario 3 ($h = 5\,\mathrm{mm}$) and (b) Scenario 4 ($h = 10\,\mathrm{mm}$).

5.3. *Effect of different sensor locations*

Scenario 4 is taken as an illustrative example to study the effect of sensor locations on the identification results, as shown in Fig. 21. It can be seen that since the damage is located at the midspan of the beam, the stripe at the damage location is brighter, thus the identification result is better when the sensor is located at midspan (Fig. 21(b)) than at the others.

5.4. *Effect of multiple damages*

In Scenario 5, two cracks are set, one of width 10 mm at $1/2L$ and the other of width 5 mm at $3/4L$, to illustrate the identification of multiple damages using the presented method, where m_1 and V_2 are considered. The deflection time histories from different sensor locations are shown in Fig. 22 and the contour plots of $|\mathrm{W}[f]|$ with sensor locations in Fig. 23.

It can be seen that all the sensors can identify the damage at midspan. However, since the damage at $3/4L$ is relatively small, the damage there cannot be easily identified when the sensor is placed at $1/4L$ and midspan while the sensor at $3/4L$ can. The locus of maximum modulus of sensor at $3/4L$ is shown in Fig. 24, and

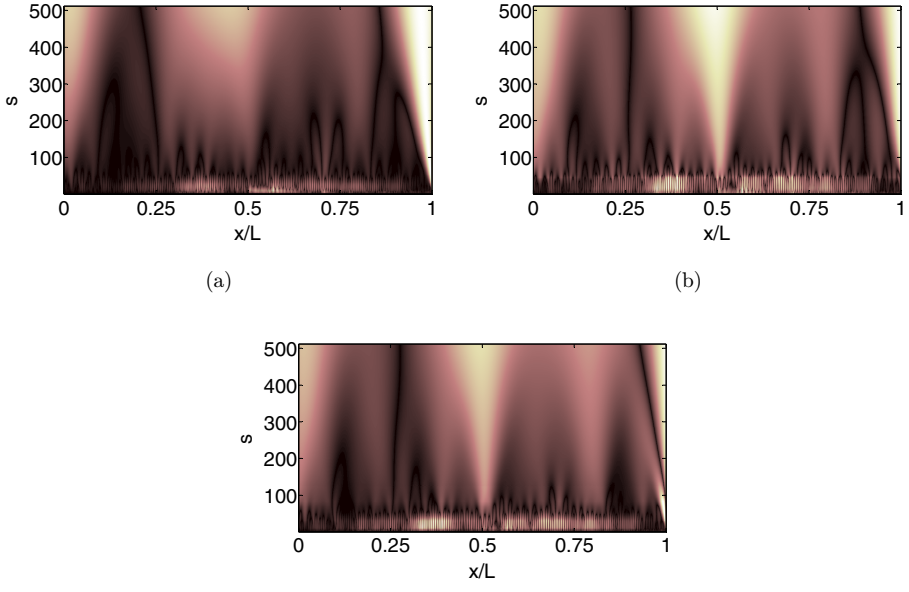

Fig. 21. Contour plots of $|\mathrm{W}[f]|$ with sensor location: (a) $1/4L$, (b) $1/2L$ and (c) $3/4L$.

the Lipschitz exponents are calculated as $\alpha_{3/4} = 1.2947 \,@\, 1/2L$ and $\alpha_{3/4} = 1.6689 \,@\, 3/4L$. Obviously, bigger damage results in smaller Lipschitz exponent at midspan.

In Scenario 6, two cracks are set, one of width 10 mm at $1/4L$ and the other of width 5 mm at $3/4L$, to illustrate the identification of multiple damages using the proposed method, where m_1 and V_2 are considered. The deflection time histories from different sensor locations of the beam are shown in Fig. 25, and the contour plots of $|\mathrm{W}[f]|$ with sensor locations in Fig. 26.

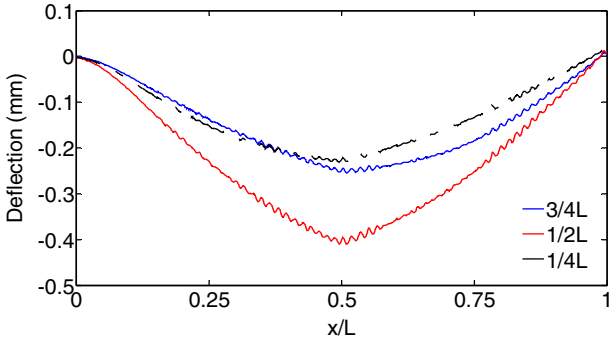

Fig. 22. Deflection time histories from different sensor locations (Scenario 5, 10 mm crack at $1/2L$ and 5 mm at $3/4L$).

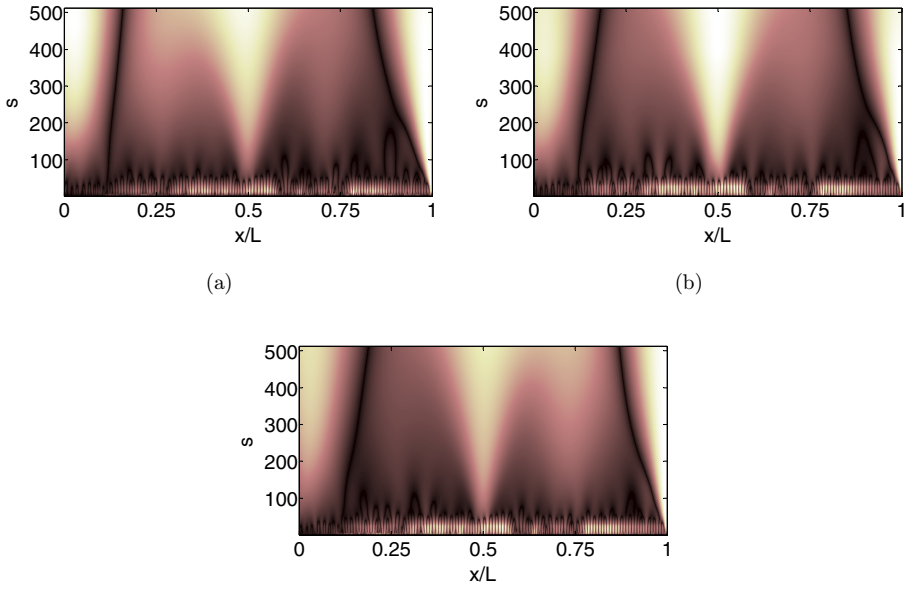

Fig. 23. Contour plots of $|\mathrm{W}[f]|$ with sensor location (Scenario 5, 10 mm crack at $1/2L$ and 5 mm at $3/4L$): (a) $1/4L$, (b) $1/2L$ and (c) $3/4L$.

From Fig. 25, it can be seen that the maximum deflection in Scenario 6 is smaller than Scenario 5 in Fig. 22, since there is a large damage at the midspan in Scenario 5, which can affect the global response. From Fig. 26, it should be noticed that the damage of $3/4L$ can easily be identified from the sensor near the damage location shown in (c), rather than in (a) and (b), which is the same as Scenario 5. The loci of maximum moduli of the response from $3/4L$ is shown in Fig. 27, and the Lipschitz exponents are calculated as $\alpha_{3/4} = 1.3743\,@\,1/4L$ and $\alpha_{3/4} = 1.5403\,@\,3/4L$. Herein, the value of $\alpha\,@\,3/4L$ is near $\alpha\,@\,3/4L$ (1.6689) in Scenario 5, since the damage

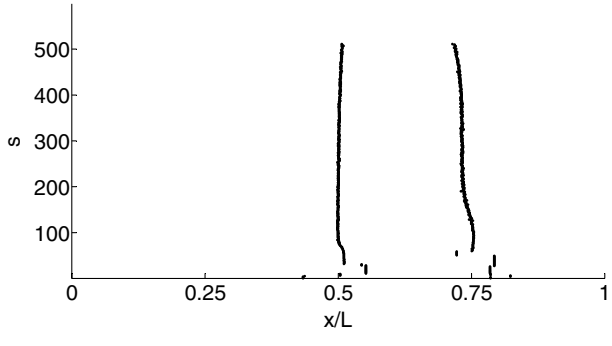

Fig. 24. Locus of maximum modulus $|\mathrm{W}[f]|_{\max}$ of deflection at $3/4L$.

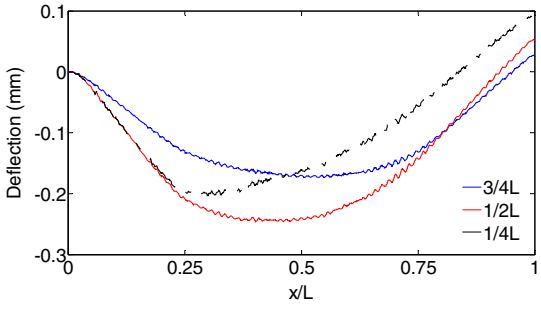

Fig. 25. Deflection time histories of different sensor locations on the beam (Scenario 6: 10 mm crack at $1/4L$ and 5 mm at $3/4L$).

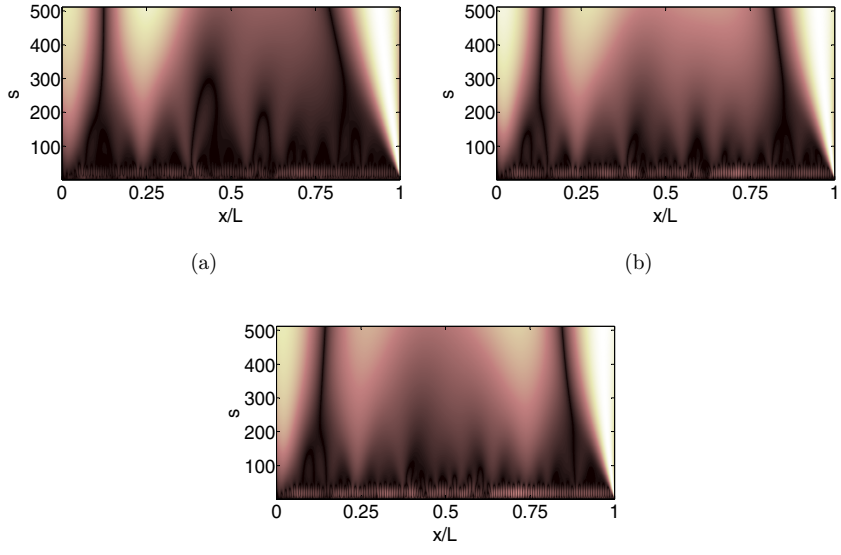

Fig. 26. Contour plot of $|\mathrm{W}[f]|$ with sensor locations (Scenario 6: 10 mm crack at $1/4L$ and 5 mm at $3/4L$): (a) $1/4L$, (b) $1/2L$ and (c) $3/4L$.

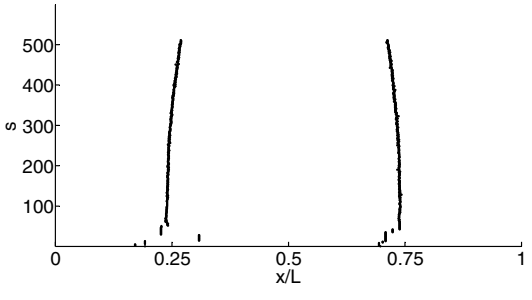

Fig. 27. Loci of maximum moduli $|\mathrm{W}[f]|_{\max}$ of deflection at $3/4L$.

degrees at $3/4L$ in both scenarios are the same, which indicates that Lipschitz exponent can be used to estimate the damage degree.

6. Conclusion

The deflection time history of one point on the damaged beam under moving load is computed numerically. The CWT and Lipschitz exponent are applied to the deflection to find the damage location, while estimating the damage degree. The feasibility of this damage identification method is verified by a model experiment. The following conclusions are drawn based on the present study:

(1) Bridge damage, whether single damage or multiple damages, can be identified by the CWT of the deflection time histories of a few sensors installed on the beam under the moving load. No information is needed of the undamaged bridge.
(2) The larger the damage degree, the smaller the Lipschitz exponent.
(3) The damage is easier to be identified by a sensor located nearby.
(4) The load velocity does not affect much the identification result. But when the velocity is too high, it is difficult to locate the damage in low scales of CWT.
(5) The load magnitude affects the deflection amplitude, but not the damage identification result.

In this paper, there is indeed certain difference between the experiment and numerical results on damage simulation, as explained in Sec. 5.1, and the comparison of numerical and experimental results just confirms the difference (in the experiment, the damage degree is larger). In Sec. 5.2, two scenarios with different damage degrees are studied, which shows that by comparison of contour plots or the Lipschitz exponents, the damage degree can be evaluated relatively, but cannot be quantified accurately. The proposed method can be used to localize the damage and roughly evaluate the damage degree. Accurate quantification of damage degree is still a problem to be researched in the future.

Acknowledgments

This study is sponsored by the State Fundamental Research Funds "973" Program (2013CB036203), the Natural Science Foundation (51308035), the Fundamental Research Funds for the Central Universities (2015RC006) and the "111" Project (B13002) of China.

References

S. W. Doebling, C. R. Farrar and M. B. Prime, A summary review of vibration-based damage identification methods, *The Shock Vibr. Digest* **30**(2) (1998) 91–105.

V. Srinivas, C. Antony Jeyasehar and K. Ramanjaneyulu, Computational methodologies for vibration-based damage assessment of structures, *Int. J. Struct. Stab. Dynam.* **13**(8) (2013) 1350043 (27 pages), doi: 10.1142/S0219455413500430.

A. K. Pandey, M. Biswas and M. M. Samman, Damage detection from changes in curvature mode shapes, *J. Sound Vibr.* **145**(2) (1991) 321–332.
M. M. M. Maia, J. M. M. Silva and R. P. C. Sampaio, Localization of damage using curvature of the frequency response functions, in *Proc. 15th IMAC*, Orlando, USA, February 1997.
H. Y. Guo and Z. L. Li, Structural multi-damage identification based on modal strain energy equivalence index method, *Int. J. Struct. Stab. Dynam.* **14**(7) (2014) 1450028 (17 pages).
S. L. Ma and L. Q. Weng, Two-stage damage identification based on modal strain energy and revised particle swarm optimization, *Int. J. Struct. Stab. Dynam.* **14**(5) (2014) 1440005 (25 pages), doi: 10.1142/S0219455414400057.
K. M. Liew and Q. Wang, Application of wavelet theory for crack identification in structures, *J. Eng. Mech.* **124**(2) (1998) 152–157.
Q. Wang and X. Deng, Damage detection with spatial wavelets, *Int. J. Solids Struct.* **36** (1999) 3443–3468.
Z. Hou, M. Noori and R. St. Amand, Wavelet-based approach for structural damage detection, *J. Eng. Mech.* **126**(7) (2000) 677–683.
Y. Y. Lee and K. M. Liew, Detection of damage locations in a beam using the wavelet analysis, *Int. J. Struct. Stab. Dynam.* **1**(3) (2001) 455–465.
B. Zhu, A. Y. T. Leung, C. K. Wong and W. Z. Lu, On-line health monitoring and damage detection of structures based on the wavelet transform, *Int. J. Struct. Stab. Dynam.* **8**(3) (2008) 367–387.
A. Alvandi, J. Bastien, E. Grégoire and M. Jolin, Bridge integrity assessment by continuous wavelet transforms, *Int. J. Struct. Stab. Dynam.* **9**(1) (2009) 11–43.
X. Q. Zhu and H. Hao, Damage detection of RC slabs using nonlinear vibration features, *Int. J. Struct. Stab. Dynam.* **9**(4) (2009) 687–709.
J. C. Hong, Y. Y. Kim, H. C. Lee and Y. W. Lee, Damage detection using the Lipschitz exponent estimated by the wavelet transform: Applications to vibration modes of a beam, *Int. J. Solids Struct.* **39**(7) (2002) 1803–1816.
S. Douka, S. Looutridis and A. Trochidis, Crack identification in beams using wavelet analysis, *Int. J. Solids Struct.* **40** (2003) 3557–3569.
S. B. Beheshti-Aval, M. Taherinasab and M. Noori, Using harmonic class loading for damage identification of plates by wavelet transformation approach, *Smart Struct. Syst. An Int'l J.* **8**(3) (2011) 253–274.
S. S. Law, X. Q. Zhu, Y. J. Tian, X. Y. Li and S. Q. Wu, Statistical damage classification method based on wavelet packet analysis, *Struct. Eng. Mech., An Int'l J.* **46**(4) (2013) 459–486.
M. A. Mahmoud, Effect of cracks on the dynamic response of a simple beam subject to a moving load, in *Proc. Institution of Mechanical Engineers Part-F Journal of Rail and Rapid Transit*, Vol. 215 (2001) pp. 207–215.
M. A. Mahmoud and M. A. Abou Zaid, Dynamic response of a beam with a crack subject to a moving mass, *J. Sound Vibr.* **256**(4) (2002) 591–603.
S. S. Law and X. Q. Zhu, Dynamic behavior of damaged concrete bridge structures under moving vehicular loads, *Eng. Struct.* **26** (2004) 1279–1293.
X. Q. Zhu and S. S. Law, Wavelet-based crack identification of bridge beam from operational deflection time history, *Int. J. Solids Struct.* **43** (2006) 2299–2317.
J. W. Zhan, H. Xia, S. C. Chen and G. De Roeck, Structural damage identification for railway bridges based on train-induced bridge responses and sensitivity analysis, *J. Sound Vibr.* **268** (2008) 103–113.

N. An, H. Xia and J. W. Zhan, Identification of beam crack using the dynamic response of a moving spring-mass unit, *Inter. Multiscale Mech. An Int. J.* **3**(4) (2010) 321–332.
A. Bagheri *et al.*, Structural damage identification of plates based on modal data using 2D discrete wavelet transform, *Struct. Engineering and Mechanics, An Int'l Journal* **40**(1) (2011) 13–28.
H. Gokdag, Wavelet-based damage detection method for a beam-type structure carrying moving mass, *Struct. Eng. Mech. An Int. J.* **38**(1) (2011) 81–97.
D. Hester and A. González, A wavelet-based damage detection algorithm based on bridge acceleration response to a vehicle, *Mech. Syst. Signal Process.* **28** (2012) 145–166.
A. Khorram, F. Bakhtiari-Nejad and M. Rezaeian, Comparison studies between two wavelet-based crack detection methods of a beam subjected to a moving load, *Int. J. Eng. Sci.* **51** (2012) 204–215.
K. V. Nguyen, Comparison studies of open and breathing crack detections of a beam-like bridge subjected to a moving vehicle, *Eng. Struct.* **51** (2013) 306–314.
J. S. Zhu and Q. Yi, Bridge-vehicle coupled vibration response and static test data-based damage identification of highway bridges, *Struct. Eng. Mech. An Int. J.* **46**(1) (2013) 75–90.
Z. H. Li and F. T. K. Au, Damage detection of bridge using responses of vehicle considering road surface roughness, *Int. J. Struct. Stab. Dynam.* **15**(3) (2015) 1450057 (28 pages).
H. Tada, P. C. Paris and G. R. Irwin, *The Stress Analysis of Cracks Handbook* (ASME Press, New York, USA, 2000).
I. Daubechies, *Ten Lectures on Wavelets*, SIAM, Philadelphia, USA (1992).
S. Mallat, *A Wavelet Tour of Signal Processing* (Academic Press, New York, USA, 1998).
S. Jaffard, Pointwise smoothness, two-microlocalization and wavelet coefficients, *Publications Matemmatiques* **35** (1991) 155–168.